Clear-sky and cloudy-sky differences in NO_2 concentrations over the United States: implications for satellite measurement applications

Daniel L. Goldberg[*,1], M. Omar Nawaz[1], Congmeng Lyu[2,3], Jian He[2,3], Annmarie G. Carlton[4], Shobha Kondragunta[5], Susan C. Anenberg[1]

[1]Department of Environmental and Occupational Health, Milken Institute School of Public Health, George Washington University, Washington, DC, USA

[2]Cooperative Institute for Research in Environmental Sciences, University of Colorado, Boulder, CO, USA

[3]NOAA Chemical Sciences Laboratory, Boulder, CO, USA

[4]Department of Chemistry, University of California - Irvine, Irvine, CA, USA

[5]NOAA NESDIS Center for Satellite Applications and Research, College Park, MD, USA

**Correspondence to*: Daniel L. Goldberg (dgoldberg@gwu.edu)

Abstract

Satellite measurements of tropospheric trace gases are often only used when there are few clouds, which screens out 20 – 70% of the data, depending on geographic region. Although clouds cause satellite data gaps, *in situ* surface measurements and model simulations can provide insight on NO_2 during cloudy conditions. Here, we intercompare surface observations, meteorological reanalysis (ERA5), satellite measurements (TROPOMI and TEMPO), and a model (WRF-Chem) during 2019 over the contiguous U.S. to quantify how NO_2 concentrations differ under clear and cloudy skies. We find that *in situ* surface NO_2 measurements are, on average, +17% larger on all days compared to clear-sky days and +36% larger during cloudy days versus clear-sky days, with a wide distribution based on geographic region and roadway proximity: largest in the Northeast U.S. and smallest in the Southwest U.S. and near major roadways. WRF-Chem simulated surface NO_2 between cloudy and clear conditions is larger than the observed differences: +59% on cloudy days vs. clear-sky days for the model. We additionally find modeled jNO_2 values are reasonable, suggesting this WRF-Chem NO_2 bias could be arising from overly rapid OH removal of NO_2 in sunlight, too slow NO_z regeneration of NO_2 in sunlight, or differing boundary layer depth biases under cloudy versus clear skies. Finally, using *in situ* NO_2 matched to provisional TEMPO data, we find the NO_2 differences between cloudy and clear conditions to be larger in the afternoon than morning. This study quantifies some of the biases in satellite measurements introduced by using only clear-sky data.

1 Introduction

Nitrogen dioxide (NO_2) is an air pollutant that adversely affects the human respiratory system (Health Effects Institute, 2022; Khreis et al., 2017) and can lead to premature mortality (Burnett et al., 2004; M. Z. He et al., 2020). NO_2 is also an important precursor for ozone (O_3) and fine particulates ($PM_{2.5}$), which also have serious health impacts. NO_x (=NO+NO_2; most NO_x is emitted as NO which rapidly cycles to NO_2) is released into the atmosphere by biogenic microbial activity in soils, high-temperature lightning, wildfires, and thermal fossil fuel combustion; in urban areas, the majority of ambient NO_2 originates from the latter (Crippa et al., 2021). Although end-of-pipe controls (Busca et al., 1998; Koltsakis & Stamatelos, 1997) can reduce the amount of NO_x emitted from fossil-fuel engines and boilers, these technologies do not recover 100% of the NO_x generation during combustion. As a consequence, NO_2 accumulates in our atmosphere and many urban areas have NO_2 concentrations that exceed the World Health Organization guideline of 5.3 ppb for an annual average (Anenberg et al., 2022).

Observing local air pollution is typically done by *in situ* surface monitors, which are spaced throughout a region with a higher density of monitors typically in areas of high population density and known pollution sources. In the United States, there are 1012 *in situ* monitoring sites measuring some combination of O_3, $PM_{2.5}$, NO_2, volatile organic compounds (VOCs), and CO (https://www.epa.gov/aqs). While the U.S. monitoring network is more comprehensive than most other countries (Martin et al., 2019), 79% of U.S. counties lack a single monitor and an additional 10% of counties have only a single monitor, leaving only 11% of U.S. counties with more than 1 monitor (Sullivan & Krupnick, 2018). Although a robust and accurate ground-monitoring network is needed, the high operating cost of these instruments can be an important barrier (Kelly et al., 2017). Spatial gaps remain in-between the regulatory monitors, and sometimes these monitors are inadequate for understanding the true ambient air pollution exposure of most U.S. residents, especially those that live and/or work several miles away from a regulatory monitor. Satellite data provide a way to fill in the gaps of the *in situ* monitoring network. Methodologies to obtain robust surface air pollutant measurement data from satellite instruments have improved dramatically in the past ten years (Bechle et al., 2015; Cao, 2023; Ghahremanloo et al., 2021, 2023; Larkin et al., 2023; Nawaz et al., 2025; Shetty et al., 2024; W. Sun et al., 2024).

NO_2 can be observed by remote sensing instruments due to its unique spectroscopic features (Vandaele et al., 1998). The Tropospheric Monitoring Instrument (TROPOMI) (Veefkind et al., 2012) has been measuring column densities of NO_2 pollution up to 7 × 3.5 km^2 before 6 August 2019 and up to 5.5 × 3.5 km^2 spatial resolution (van Geffen, 2016) since 6 April 2019. Because of TROPOMI's higher spatial resolution over predecessor instruments, such as the Ozone Monitoring Instrument (OMI) (24 × 13 km^2 at nadir) (Levelt et al., 2018), TROPOMI has ~50 daily satellite pixel measurements within a typical city (~1000 km^2) during clear skies, while OMI may have only 1-3 daily measurements within the borders of each city. This increased measurement capacity within a city allows us to discern spatial variability undetectable by previous instruments.(de Foy et al., 2009; K. Sun et al., 2018)

Level 2 satellite NO_2 measurements – which are retrieved from observed NO_2 spectra using geophysical and model-based assumptions – are of the tropospheric column. In many cases, NO_2 column measurements are strongly correlated

with the spatial patterns of surface NO_2 concentrations (Acker et al., 2025; Harkey & Holloway, 2024; Kim et al., 2024) and surface NOx emissions (Goldberg et al., 2024). For TROPOMI, studies have shown a strong correlation between tropospheric column measurements and collocated surface NO_2 for both the 13:30 average ($r^2 = 0.67$) and the 24-hour average ($r^2 = 0.68$) (Goldberg et al., 2021; Kerr et al., 2023). However, there are rare instances in which NOx emissions and NO_2 enhancements stay aloft and do not affect the surface; these are often situations associated with lightning NOx (Nault et al., 2017), wildfire NOx (Jin et al., 2021; Lin et al., 2024), and aircraft NOx (Maruhashi et al., 2024). In these instances, it can be difficult to determine if the column NO_2 enhancements are also leading to surface NO_2 enhancements. These misinterpretations are more likely to occur over rural regions and/or individual days, as upper-tropospheric NO_2 enhancements near urban regions often dwarf NO_2 enhancements within the boundary layer especially over monthly or longer timescales (Goldberg et al., 2022).

Satellite measurements of trace gases are typically only used when there are few or no clouds; this is often referred to as the clear-sky bias of satellite data. In the U.S., this results in 20 – 70% of the satellite data being filtered out depending on geographic region. The clear-sky bias affects NO_2 moreso than other trace gases (such as CO and CH_4) because NO_2 is very photochemically active in the presence of strong sunlight; its effective lifetime during summer daytime is 2 – 7 hours (F. Liu et al., 2016) and conversely can be up to 30 hours during winter daytime (Kenagy et al., 2018). The speed at which it transforms into other chemical species is determined by the irradiation, ambient temperature, and oxidative capacity (Laughner & Cohen, 2019; Shah et al., 2020). More specifically, strong irradiation creates the OH radical which can react with NO_2 to create HNO_3 – a major terminal sink of NO_2 – and also accelerates the photolysis of NO_2 into NO and $O(^3P)$ leading to an accumulation of O_3 in the presence of VOCs; without VOCs, NO_2 cycles more rapidly to NO. Warm temperatures increase biogenic VOC emissions and VOC can react with NO_2 directly to create organic nitrates (e.g., peroxyacetyl nitrates and alkyl nitrates) (Zare et al., 2018) which act as a temporary sink of NO_2. Another daytime terminal sink for NO_2 is dry deposition; while this removal mechanism is often secondary to photochemical loss in urban environments and is not directly affected by sunlight, it is indirectly affected as cloudy conditions are often associated with increased relative humidity and shallower boundary layer depths, both of which increase dry deposition fluxes. Therefore, increased NO_2 dry deposition fluxes in cloudy conditions could offset some of the decreased NO_2 photochemical loss rates. The net result is that NO_2 concentrations are typically larger during cloudy conditions (Geddes et al., 2012).

However, outside of the Geddes et al. (2012) study, little has been done to observationally quantify the bias of NO_2 being larger during cloudy conditions particularly because there are no column measurements to validate the satellite during cloudy conditions. With that said, there are surface *in situ* measurements during cloudy conditions that can give us an idea of how the clear-sky bias may affect the estimate of surface concentrations. In this project, we intercompare surface observations, meteorological reanalysis (ERA5), satellite measurements (TROPOMI and TEMPO), and a model (WRF-Chem) under clear and cloudy skies to better quantify the amount of surface and column bias of NO_2 concentrations that is being introduced when clouds are screened from the satellite data. Our analysis is focused on the United States during 2019 due the high density of *in situ* monitors and availability of high-

resolution regional chemical transport models. The motivation of this project is to determine what the scientific community may be missing when excluding clouds from satellite-based NO_2 analyses.

2 Methods

2.1 EPA AQS Data

Hourly *in situ* NO_2 measurements were obtained from the pre-generated EPA Air Quality System (AQS) database: https://aqs.epa.gov/aqsweb/airdata/download_files.html. These routine measurements are operated and maintained by various state and federal agencies. 91% of the "NO_2" measurements in 2019 were acquired through a chemiluminescence technique which converts NO_2 and unintendedly some NO_z species – such as alkyl nitrates, peroxynitrates (PAN), and nitric acid (HNO_3) – to NO using a heated molybdenum converter; the NO is measured by quantifying the luminesce of NO when reacted in excess O_3 (Dickerson et al., 2019). Lamsal et al. (2008) suggested a correction factor for converting midday chemiluminescence NO_2^* (=NO_2 + unintended NO_z) measurements to NO_2 using modelled information of PAN, alkyl nitrates, and HNO_3. In Equation 1, we show the Lamsal et al. (2008) correction factor with a modification to exclude alkyl nitrates which are not explicitly included in our WRF-Chem simulation.

$$[NO_2]^* = F_{int} \times [NO_2] \quad \text{where } F_{int} = \frac{[NO_2]+0.95[PAN]+0.35[HNO_3]}{[NO_2]} \tag{1}$$

Typically, correction factors are in the range of ~1.0 for fresh urban plumes and can be as large as ~3.0 for rural areas during summer, with averages typically in the 1 – 1.5 range for moderate and very polluted regimes, and are important to use for model vs. monitor intercomparisons (Kuhn et al., 2024; Lamsal et al., 2008; Poraicu et al., 2023). Other methods to measure *in situ* NO_2 include Cavity Attenuated Phase Shift (Kebabian et al., 2008) and Laser Induced Fluorescence (Thornton et al., 2000), but these methods are less common (9% of all NO_2 monitors in 2019).

Annual and seasonal averages at 13:30 local standard time (between 13:00 – 14:00) of the *in situ* data were considered valid and used if more than 75% of the days of the year/season had valid data. There were 449 monitoring locations in 2019 in the U.S. that achieved these criteria for an annual average, which equates to 1 monitor per ~730,000 U.S. residents. For the baseline analysis, we further remove data from the 75 monitoring locations (17% of the locations) that are classified as "near-road" by the EPA, which means that they are installed within 20 m from major interstates since these *in situ* measurements are not representative of a ~20 km^2 satellite pixel measurement; we include the "near-road" NO_2 monitoring data in sensitivity analyses. NO_2 measurements between cloudy and clear-sky days are intercompared using the normalized mean change (NMC) as described in Equation 2, where $\bar{x}$ and $\bar{y}$ are means of the two datasets being analyzed.

$$NMC(\%) = 100 \times \left(\frac{\bar{y}-\bar{x}}{\bar{x}}\right) \tag{2}$$

2.2 Satellite NO_2 Instruments

NO_2 slant column densities are derived from radiance measurements in the 405 – 465 nm spectral window of the UV-VIS-NIR spectrometer (van Geffen et al., 2021; Nowlan et al., 2025). Satellite instruments observe NO_2 by comparing observed spectra with a reference spectrum to derive the amount of NO_2 in the atmosphere between the instrument and the surface; this technique is called differential optical absorption spectroscopy (DOAS) (Platt, 1994). Tropospheric vertical column density data, which represent the vertically integrated NO_2 concentrations between the surface and the tropopause, are then calculated by subtracting the stratospheric portion and then converting the tropospheric slant column to a vertical column using an air mass factor (AMF) (Boersma et al., 2011). The AMF is a unitless quantity used to convert the slant column into a vertical column and is a function of the satellite viewing angles, solar angles, the effective cloud radiance fraction and pressure, the vertical profile shape of NO_2 provided by a chemical transport model simulation, and the surface reflectivity (Lorente et al., 2017; Palmer et al., 2001).

2.2.1 TROPOMI

TROPOMI was launched by the European Space Agency (ESA) on 13 October 2017, and data from the instrument became available on 30 April 2018, after an approximately 6-month calibration period. The satellite follows a sun-synchronous, low-earth (825 km) orbit with an equator overpass time of approximately 13:30 local solar time. TROPOMI measures total column densities of several trace gases: NO_2, HCHO, O_3, CO, CH_4, among others. At nadir, pixel sizes are 3.5×7 km^2 (modified to 3.5×5.5 km^2 on August 6, 2019) with the edges having slightly larger pixels sizes (~14 km wide) across a 2600 km swath, equating to 450 rows (van Geffen et al., 2020).

For our analysis we use the TROPOMI NO_2 version 2.4 (V2.4) re-processed algorithm during Jan 1, 2019 – Dec 31, 2019. We also conducted a sensitivity study using the version 2.3.1 (V2.3.1) algorithm. The TROPOMI NO_2 V2.4 product has a documented median low bias of -34.8% in moderately polluted locations (when NO_2 measurements are between $3 – 14 \times 10^{15}$ molec/cm^2) when compared to a MAX-DOAS network (Lambert et al., 2023). Some of this low bias is due to the operational AMF which uses a $1° \times 1°$ model to assume vertical shape profiles; when vertical shape profiles from a regional model are instead used, the bias decreases to between -1% and -23% (Nawaz et al., 2024, Judd et al., 2020, Tack et al., 2021). Prior work has demonstrated a strong correlation between TROPOMI NO_2 column measurements and NO_2 surface concentrations in urban areas (Demetillo et al., 2020; Dressel et al., 2022; Goldberg et al., 2021; Nawaz et al., 2025). For our baseline, we screened TROPOMI pixels for quality assurance flag values greater than 0.75, and conduct a sensitivity analysis of filtering only with a cloud radiative fraction filter of 0.5. The cloud radiative fraction is calculated from the O_2 A-band using the FRESCO-S algorithm. Due to differences in wavelength between the O_2 A-band and the NO_2 retrieval window, the cloud fraction retrieved in the O_2 A-band is not exactly representative for the cloud fraction in the NO_2 window, but it is similar.

The filtered data were re-gridded to a $0.01° \times 0.01°$ resolution, to create a custom “Level-3” data product (Goldberg et al., 2021) during cloud-free and cloudy conditions. Single pixel TROPOMI tropospheric vertical column NO_2 uncertainties have been quantified to be between 25 – 50% under clear skies and this uncertainty is dominated by

uncertainty in the tropospheric air mass factor (Glissenaar et al., 2025; S. Liu et al., 2021; Rijsdijk et al., 2025); uncertainties of measurements with cloud fractions > 0.5 are larger. Oversampled NO_2 measurements over monthly and annual timeframes (10s - 100s of measurements) have a smaller amount of uncertainty, approximately 10 – 20 % depending on location and season (Glissenaar et al., 2025) .

2.2.2 TEMPO

TEMPO was launched by SpaceX on 7 April 2023 and is hosted on Maxar Intelsat 40e. Data from the instrument became available on 2 August 2023, after an approximately 4-month dry-out, cool-down, and calibration period. The satellite is in geostationary orbit centered over the United States with north-south coverage extending from Mexico City (~17°N) to the Canadian Oil Sands (~58°N) and east-west coverage from Puerto Rico to the Pacific coast. TEMPO operationally measures total column densities of NO_2, HCHO, and O_3 with additional products forthcoming. At nadir, pixel sizes are 4.75 × 2 km^2 with the North-east and North-west edges having slightly larger pixels sizes. The instrument observes the full east-west swath approximately once every hour.

For our analysis we use the TEMPO NO_2 version 3 algorithm during 2 Aug 2023 – 31 Aug 2024. The data was filtered to include pixels only where the effective cloud fractions are less than 0.15 and the main data quality flags are equal to 0. The filtered data was re-gridded to a 0.01° × 0.01° resolution, to create a custom "Level-3" data product (Goldberg et al., 2021) during cloud-free and cloudy conditions. Single pixel TEMPO tropospheric vertical column NO_2 uncertainties can be assumed to be similar to the uncertainty of TROPOMI measurements (Glissenaar et al., 2025), which are between 25 – 50% under clear skies for individual pixels, and 10 – 20% for oversampled averages; future work will better quantify the uncertainties of TEMPO NO_2 measurements.

2.3 ERA5 Re-analysis

We intercompare the cloud radiative fractions from TROPOMI to the ERA5 re-analysis (Hersbach et al., 2020) of total cloud fractions in the early afternoon (18Z for Eastern Time, 19Z for Central Time, 20Z for Mountain Time, 21Z for Pacific Time), which approximates the overpass time of TROPOMI over the contiguous United States. The ERA5 total cloud fraction is a unitless quantity representing how much of a grid cell is covered by a cloud (e.g., condensed water vapor) at any vertical level of the atmosphere and does not differentiate between the optical properties of those clouds. The ERA5 re-analysis data are reported at a 0.25° × 0.25° spatial resolution and the cloud fractions are interpolated, using bilinear interpolation, to the 0.01° × 0.01° oversampled TROPOMI NO_2 grid.

2.4 WRF-Chem

The Weather Research and Forecasting with Chemistry (WRF-Chem) model was run at 12 km × 12 km over the Continental U.S. for all days of 2019: 1 January 2019 – 31 December 2019 as described in He et al. (2024). For anthropogenic emissions, the Fuel-based Inventory of Vehicle Emissions (FIVE) was used to provide on-road and off-road mobile emissions, the Fuel-based Oil and Gas (FOG) inventory was used for emissions associated with oil and natural gas production, power plant emissions were provided by Continuous Emissions Monitoring Systems (CEMS),

and all other anthropogenic emissions were obtained from the 2014 or 2017 National Emissions Inventory (NEI). Biogenic emissions were estimated using Biogenic Emissions Inventory System (BEIS) version 3.13. Gas-phase chemistry was from the RACM_ESRL_VCP scheme. Boundary conditions were provided from the Realtime Air Quality Modeling System (RAQMS, http://raqms-ops.ssec.wisc.edu/) developed by the University of Wisconsin-Madison. The cloud fractions used in this project are from the total cloud fraction "CLDFRA" variable.

3 Results

3.1 CONUS Cloud Patterns

We first conduct an analysis of cloud patterns across the contiguous United States, and inter-compare clear-sky days estimated by TROPOMI, the ERA5 re-analysis, and the WRF-Chem model (Figure 1). For TROPOMI, we define clear skies as the percentage of days with qa_value > 0.75, which almost exclusively filters based on cloud fractions <0.5; cloud-free snow-covered scenes typically have a qa_value > 0.75 (Eskes et al., 2022). For ERA5 and WRF-Chem, we define clear skies as the percentage of days with the total cloud fractions <0.5. ERA5 and WRF-Chem have similar clear-sky spatial patterns as TROPOMI but show systematically lower amounts of clear-skies by 8%. The small systematic difference between TROPOMI and ERA5 when filtering for cloud fractions at 13:30 is likely driven by how optically thin cirrus-like clouds are handled; for TROPOMI these are being observed based on optical properties and therefore optically thin clouds are not assumed to be a cloud, whereas in weather models (ERA5 and WRF-Chem) these are being computed as vertical layers in the atmosphere with condensed water vapor. Overall, there is very strong agreement between the three datasets in the estimation of clouds giving us confidence that TROPOMI, ERA5, and WRF-Chem are all good estimators of daily clear-sky amounts.

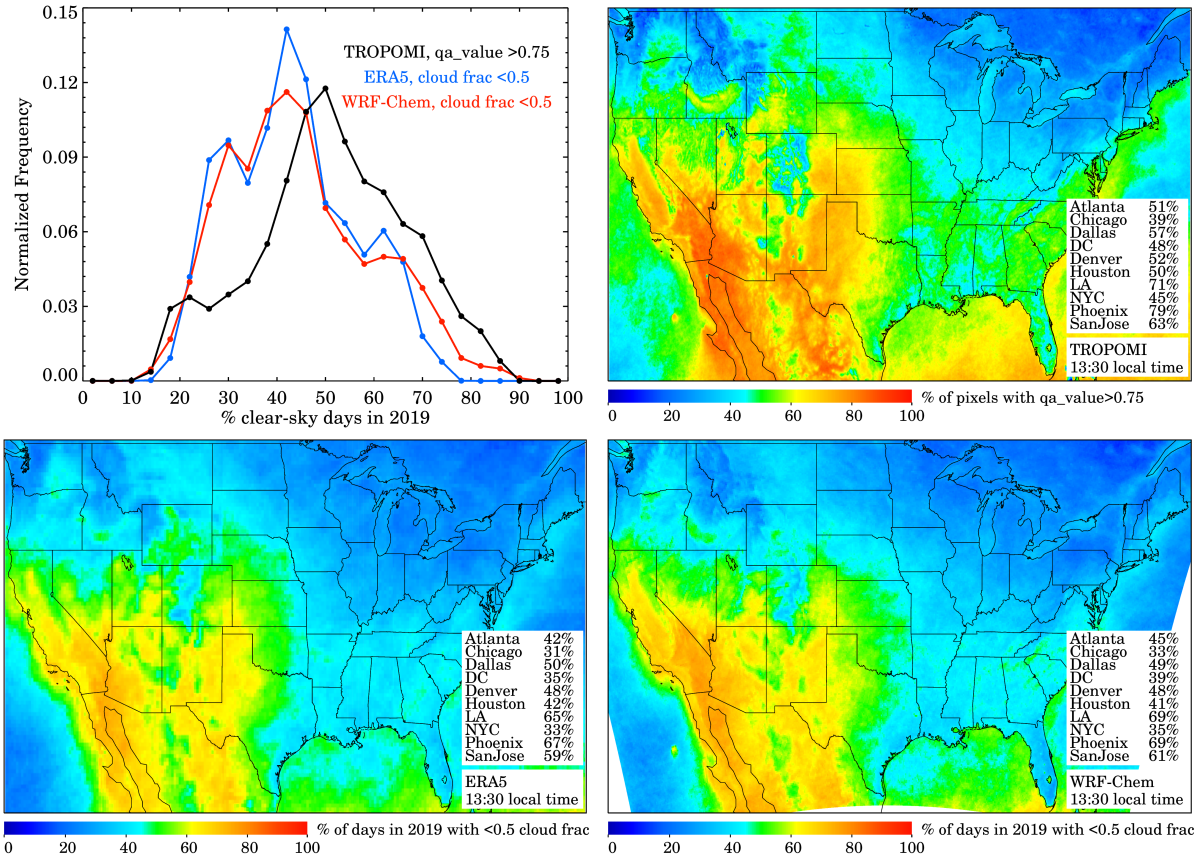

Figure 1. Percentage of clear-sky days over the contiguous U.S. during 2019 from the TROPOMI NO_2 V2.4 product, ERA5 re-analysis, and WRF-Chem. (Top left) Normalized frequency diagram of the binned percentage of clear sky days for the three products. (Top right) Percentage of days in which the qa_value of the TROPOMI NO_2 V2.4 measurement was greater than 0.75. (Bottom left) Percentage of days in which the total cloud cover (tcc) from the ERA5 was less than 0.5. (Bottom right) Percentage of days in each grid cell in which the total cloud fraction from the WRF-Chem was less than 0.5

For the remainder of this project, we define "clear sky" based on the TROPOMI NO_2 retrieval and use days with observations exceeding a qa_value of 0.75. According to TROPOMI – which is the only true observational dataset – the Southwest U.S. has the most amount of clear-sky days per year (~80% of days at 13:30 local time), while the interior Northeast U.S. and coastal Northwest has the fewest (~30% of days at 13:30 local time). The major U.S. city with the most clear-sky days is Phoenix (79% of days), while the major U.S. city with the least clear-sky days is Seattle (29% of days).

Annualized spatial cloud patterns are similar throughout the daylight hours with marginally more clear skies in the morning hours especially in the eastern U.S (Figure S1). Despite this, clouds are often transient, and there are opportunities to observe a clear sky measurement at a different hour of the day if the 13:30 observation is obstructed by clouds. In Figure 2, we demonstrate that between 68% – 93% of days have a clear sky measurement during any hour of the daytime as compared to the 33 – 69% range at 13:30.

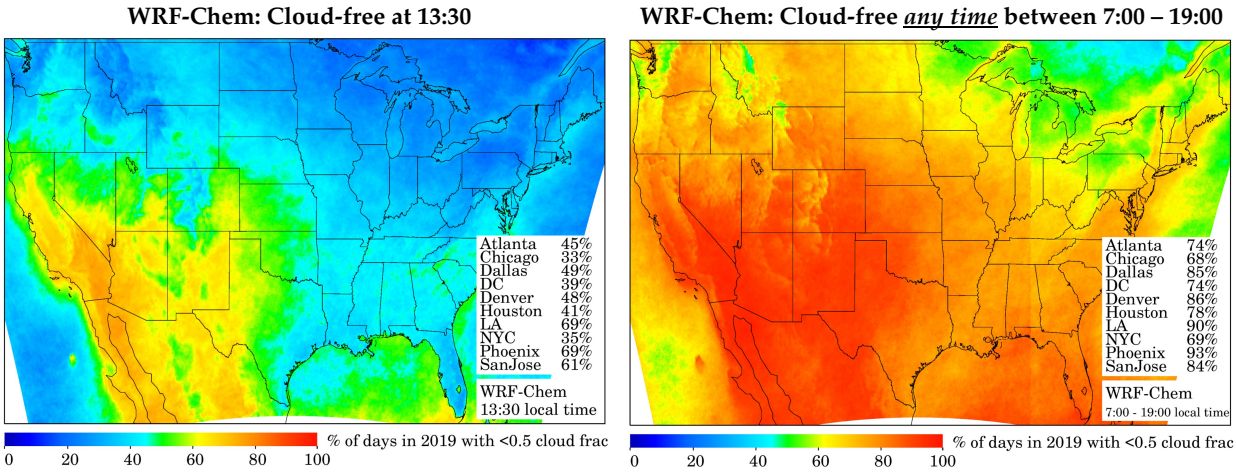

Figure 2. Percentage of days over the contiguous U.S. during 2019 with cloud fractions less than 0.5 as simulated by WRF-Chem at various local times: (Left) 13:30, (Right) any time between 7:00 – 19:00.

3.2 Surface NO_2: Clouds vs. No Clouds

We then link whether TROPOMI is observing a clear sky or not (i.e., qa_value > 0.75) to the daily *in situ* ground-level NO_2 observations to determine how clouds are affecting surface NO_2 concentrations (hereafter referred to as surface NO_2). In Figure 3, we show that surface NO_2 at 13:30 local time is +12.9% larger (NMC = normalized mean change) [–3.8% (10^{th} percentile), +32.1% (90^{th} percentile)] on days with clouds at 13:30 compared to the annualized 13:30 average when all days of data are included. We also note the very strong correlation between the NO_2 on cloudy days and all days, which suggests that the presence of clouds drives a systematic change from the mean rather than a random change. We next show that the NO_2 during the average of all days is +17.2% larger [–1.8%, +38.7%] than on days with only clear skies. We further show that surface NO_2 at 13:30 is +36.0% larger [–6.1%, +72.9%] on days with clouds compared to days with clear skies.

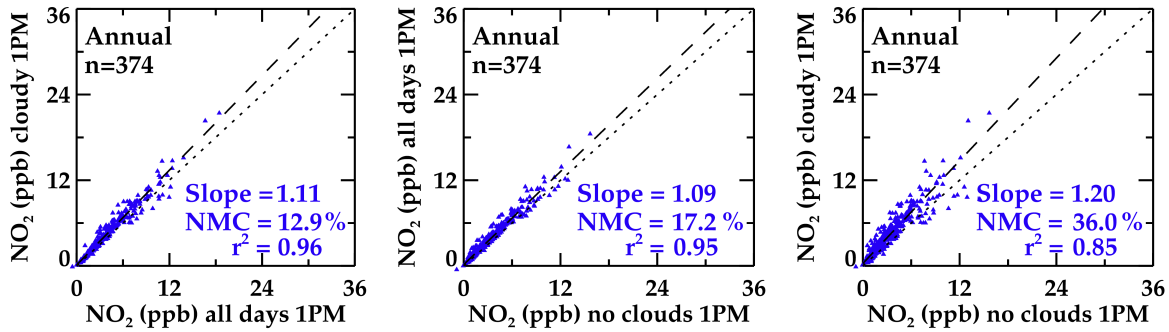

Figure 3. Scatterplots intercomparing annualized surface NO_2 from the EPA AQS at 13:30 local time during all days, cloudy days, and cloud free days. (Left) Annualized surface NO_2 during cloudy days compared to annualized surface NO_2 during all days. (Center) Annualized surface NO_2 during all days compared to annualized surface NO_2 during cloud free days. (Right) Annualized surface NO_2 during cloudy days compared to annualized surface NO_2 during no cloud. Each scatter point corresponds to each of the 374 measurement stations. A "cloudy" vs "no cloud" day is determined via the qa_value of 0.75 from the TROPOMI NO_2 V2.4 product.

The difference in surface NO_2 between cloudy and clear sky days can vary dramatically based on geographic region and proximity to a major roadway (Table 1). For the purposes of the sensitivity study, we focus on the cloudy versus cloud free days, while the directional changes of "cloudy versus all days" and "all days versus no clouds" values are similar (Tables S1 & S2).

Table 1. Slope, r^2, Normalized Mean Change (NMC), and number of sites of the "cloudy vs. no clouds" bias by further filtering out AQS data using various additional sensitivity analyses. Tables S1 & S2 show the sensitivity analyses for the "cloudy vs. all days" bias, and "all days vs. no clouds" bias respectively.

	Slope	r^2	Normalized Mean Change (%)	# sites of monitoring sites used
Baseline (V2.4)	1.20	0.85	+36.0%	374
V2.3.1	1.18	0.86	+40.4%	374
V2.4 crf<0.5	1.25	0.83	+80.8%	373
V2.4 all sites	1.05	0.90	+32.7%	449
V2.4 near road only	0.89	0.84	+15.9%	76
V2.4 no chemiluminescence	1.20	0.87	+53.1%	26
V2.4 Summer only	1.17	0.86	+23.8%	366
V2.4 Winter only	1.14	0.82	+27.8%	373
V2.4 Spring only	1.28	0.88	+31.9%	364
V2.4 Fall only	1.07	0.77	+30.9%	359
V2.4 North only	1.31	0.89	+41.5%	217
V2.4 South only	0.98	0.82	+28.5%	157
V2.4 NorthEast only	1.36	0.93	+61.7%	106
V2.4 SouthEast only	1.27	0.94	+33.8%	73
V2.4 NorthWest only	1.12	0.88	+22.2%	111
V2.4 SouthWest only	0.91	0.79	+23.9%	84
V2.4 lowPopDensity only	1.34	0.86	+36.3%	216
V2.4 highPopDensity only	1.13	0.76	+37.5%	167
V2.4 lowRoadDensity only	1.19	0.82	+33.6%	216
V2.4 highRoadDensity only	1.18	0.80	+40.8%	165

First, we find that NO_2 during cloudy days is larger in the northern U.S. (+41.5%) than the southern U.S. (+28.5%) and largest in the Northeast U.S (+61.7%) (Figure 4); for this analysis, 37°N is the dividing latitude between North and South, 100°W is the dividing longitude between East and West. Although the calculated cloudy versus no cloud change is independent of the number of days of clear-skies, areas of perpetually cloudy skies also have cooler temperatures, decreased photolysis, and shallower boundary layers which could cause much larger NO_2 on cloudy days. Interestingly, the Phoenix and Salt Lake City areas – two areas with large number of days with clear skies – also have a relatively large difference between cloudy and clear sky days demonstrating that the bias is independent of the number of days with clear skies. However, the *annualized* difference between cloudy and clear sky days in the Southwest U.S. is modest (+4.8%) (Table S1) because there are fewer individual days affected by clouds. Approximately 13% of monitoring sites, mostly concentrated in the Los Angeles and San Diego areas, have lower NO_2 on cloudy days, and this may be driven by enhanced westerly winds on cloudy days bringing in cleaner marine air more than offsetting the photochemically driven larger NO_2 on cloudy days. Overall, while there are a few locations with lower NO_2 on cloudy days, 87% of locations exhibit larger NO_2 on cloudy days and this is driven by the slower photochemistry on these days.

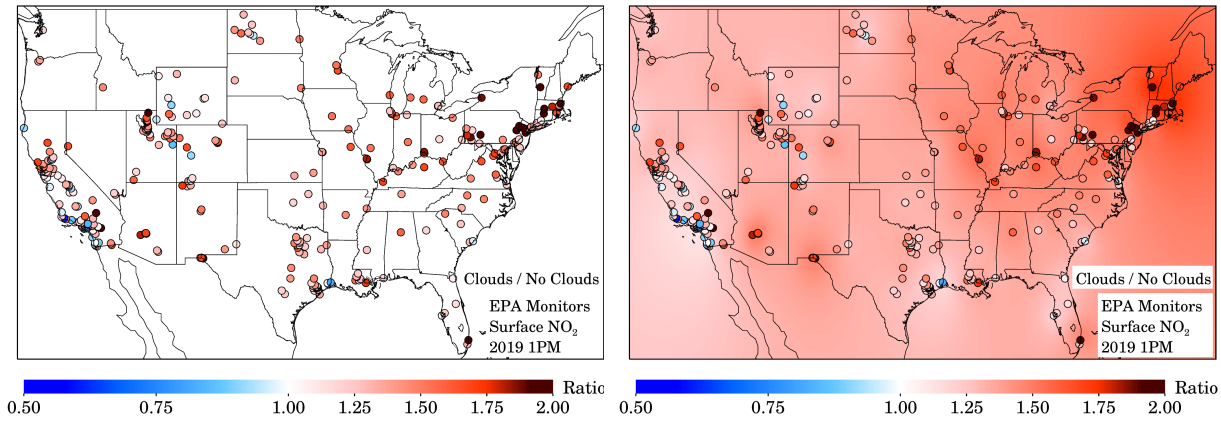

Figure 4. (Left) Ratio of the annualized surface NO_2 during cloudy and cloud free days at the EPA AQS sites not classified as "near-road". (Right) Same image but with an inverse distance weighting underlaid to infer geographic distribution of the ratio.

Proximity to roadways and large sources of NOx is another driver of whether a location will experience a small – but generally still positive – difference in NO_2 on cloudy and clear sky days. For areas in close proximity to roadways (i.e., the near-road sites) (n=76), the difference in NO_2 between cloudy and clear sky days is weaker: a smaller positive change (+15.9%) and only 77% of sites displaying a positive mean change, which is less than the difference at all other NO_2 monitoring locations (+36.0%).

We find that seasonal effects on the differences in NO_2 between cloudy and clear days are modest. The NO_2 on cloudy days in the Spring is largest and marginally smaller in other seasons. Other factors that were not associated with strong changes to the differences in NO_2 between cloudy and clear days bias are: the version of the TROPOMI NO_2 algorithm,

whether the site was using a chemiluminescence or Cavity Attenuated Phase Shift measurement technique, and population / roadway density within a 0.5° radius.

3.3 TROPOMI NO_2: Clouds versus No Clouds

We then compare TROPOMI NO_2 measurements under varying sky conditions to understand how the retrieved NO_2 columns differ under cloudy and clear-sky conditions, but not to answer how they actually differ. For this exercise, we filter the TROPOMI NO_2 data strictly based on cloud radiative fraction (crf). Although it is recommended for most applications to use data when the crf <0.5, sometimes measurements are usable in the presence of optically thick clouds (i.e., crf >0.5). In Figure 5, we average TROPOMI NO_2 measurements below and above a crf = 0.5 threshold to gain an understanding of how TROPOMI column NO_2 measurements intercompare in the presence and lack of optically thick clouds. In the figure we show the tropospheric vertical columns on the top row, and tropospheric slant columns in the middle row, which have been interconverted using the tropospheric air mass factor shown on the bottom row. As discussed in Section 2.2.1, the tropospheric air mass factor can be a large source of uncertainty when calculating tropospheric vertical columns from slant columns (Glissenaar et al., 2025; S. Liu et al., 2021; Rijsdijk et al., 2025).

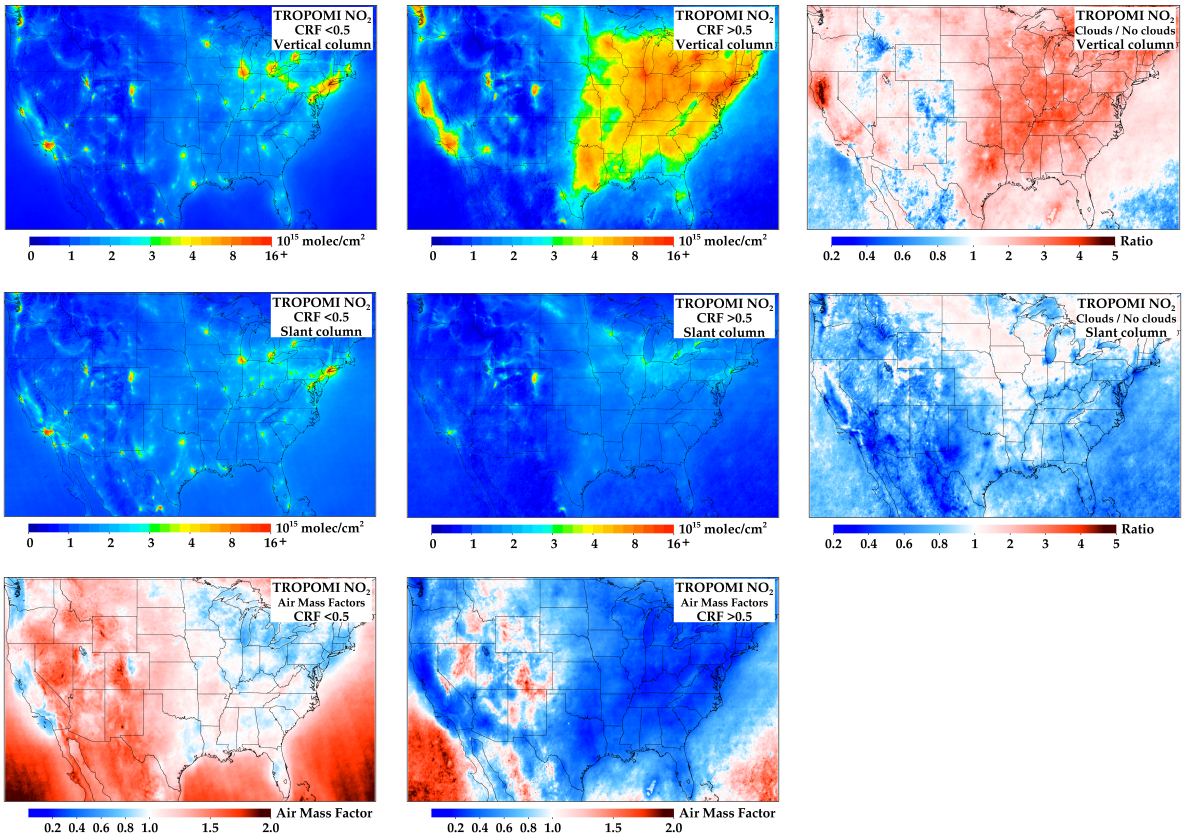

Figure 5. (Left column) Annual 2019 TROPOMI NO_2 filtered using only a cloud radiative fraction (crf) filter less than 0.5. (Center column) Annual 2019 TROPOMI NO_2 filtered using only a crf filter greater than 0.5. (Right column) Ratio between the two annual averages. (Top row) Vertical tropospheric column NO_2 data. (Center row) Slant tropospheric column NO_2 data. (Bottom row) Tropospheric air mass factors.

In Figure 5, we demonstrate that the vertical column NO_2 spatial patterns in the presence of clouds are much different in magnitude than the slant column NO_2 whereas the vertical column NO_2 spatial patterns in the absence of clouds are similar to the slant column NO_2. This is primarily driven by the assumed scattering weights in the retrieval. During cloudy scenes, scattering and reflection by clouds reduce the satellite's sensitivity to near-surface NO_2, leading to smaller air mass factors as shown. Also, during measurements when the crf >0.5, the uncertainty of the TROPOMI vertical column measurements rises, and this is driven by the difficulty in calculating the air mass factor in the presence of clouds; in addition to needing to know the vertical NO_2 profile for its calculation, we also need to know the pressure level and thickness of the clouds. Such errors can generate nonlinear responses. This analysis confirms that the assumed air mass factor is the driving factor causing the retrieved differences in the tropospheric vertical column NO_2 between clear and cloudy sky days, as the slant tropospheric column NO_2 is smaller during cloudy skies due to a lack of instrument sensitivity to the surface during cloudy conditions. Therefore, special care should be used when interpreting retrieved tropospheric satellite measurements in the presence of clouds.

Qualitatively, the ratio of the column NO_2 with and without clouds is spatially similar to the ratio from the AQS analysis – with the largest ratios occurring in the Northeast U.S and smallest ratios occurring in the Southwest U.S. However, quantitatively, the column ratio observed by TROPOMI is much larger in magnitude in the eastern U.S. than the surface ratio observed at the AQS surface sites. It is difficult to determine whether the quantitative magnitude is correct because there are no ground-based instruments to accurately measure column NO_2 in the presence of clouds.

3.4 WRF-Chem NO_2: Clouds vs. No Clouds

We then compare the differences in NO_2 between cloudy and clear days observed by the EPA AQS surface network to the differences in NO_2 between cloudy and clear days of surface NO_2 simulated by WRF-Chem. The 13:30 local time differences in NO_2 between cloudy and clear days of surface NO_2 in WRF-Chem (+58.7%) is substantially larger than from the AQS observations (+36.0%) during collocations. This directional change is consistent among all geographic regions suggesting that NO_2 concentrations are too responsive to sunlight in WRF-Chem.

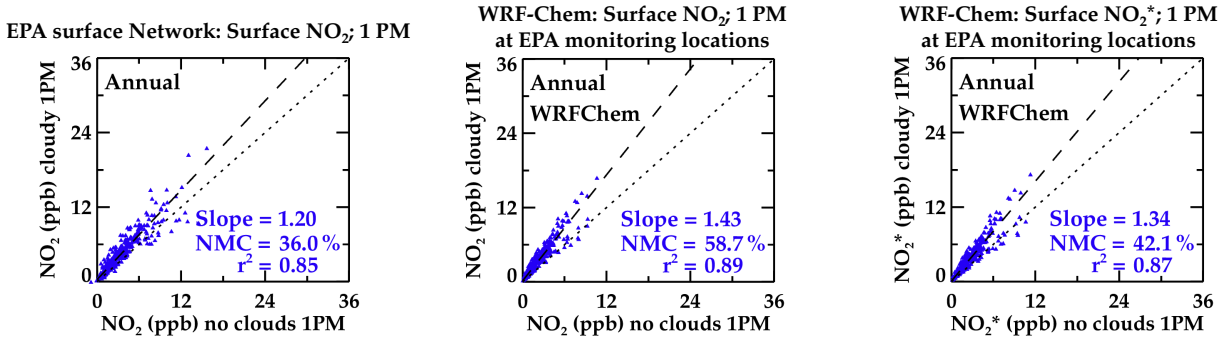

Figure 6. Scatterplots intercomparing annualized surface NO_2 at 13:30 local time during cloudy days vs. cloud free days. (Left) EPA AQS data which is a repeat of Figure 3c. (Center) WRF-Chem collocated with the AQS monitoring sites, and using the WRF-Chem cloud filter in lieu of the TROPOMI cloud filter. (Right) WRF-Chem collocated with the AQS monitoring sites, comparing NO_2* instead of NO_2.

There could be several reasons for this discrepancy. First, 91% of monitors in the EPA monitoring network measure using the chemiluminescence method, NO_2^*, which quantifies NO_2 in addition to some fraction of PAN, alkyl nitrates, and HNO_3. The latter is problematic because the $NO_2 + OH \rightarrow HNO_3$ reaction is a photochemically-driven pathway for NO_2 during daytime and if HNO_3 is additionally being measured then this would appear to buffer photolytically driven changes. We further conducted a sensitivity test in WRF-Chem and found that the NMC is only +42.1% down from +58.7% when a chemiluminescence correction factor from Equation 1 is used (Figure 6c), indicating that some of the perceived differences between WRF-Chem and EPA monitors could be due to monitor interferences from PAN and HNO_3. Second, it is possible that radical concentrations (OH, HO_2, and/or RO_2) in WRF-Chem are fluctuating improperly in the presence of and lack of clouds (Duncan et al., 2024) causing NO_2 to either be removed too rapidly in the model or regenerated too slowly. Third, there might be insufficient photolysis of organic nitrates and/or particulate nitrates in the model which could buffer NO_2 photolysis-related changes; recent work has suggested that particulate nitrate can meaningfully photolyze back to NO_2 (Sarwar et al., 2024; Shah et al., 2024). Fourth, WRF-Chem may not simulate PBL depth properly and may have different biases during cloudy and clear sky conditions (Hegarty et al., 2018; Kuhn et al., 2024; X. Liu et al., 2023). For example, if the predicted PBL is too shallow during cloudy conditions, this could be a contributing factor to the simulated surface NO_2 bias. Errors in surface jNO_2 do not appear to be a primary driver of the cloudy versus clear sky disagreements as the jNO_2 values from WRF-Chem seem reasonable as compared to UV-B measurements from the NOAA Surface Radiation Budget (SURFRAD) monitoring network (Figure S4) and is consistent with other work showing small biases in jNO_2 in WRF-Chem (Ryu et al., 2018). Follow-up work will address some of these shortcomings by adding particulate nitrate photolysis into the chemical mechanism and evaluating PBL depths during cloudy conditions using ceilometers.

We can then use WRF-Chem as a transfer standard to suggest how column NO_2 may change in relation to the surface NO_2, and we find that the relative change in column NO_2 and surface NO_2 in response to clouds are very similar (Figure 7). This makes intuitive sense because most NO_2 over the contiguous U.S. is located within the boundary layer, and typically clouds (if they exist) are located at the top of the boundary layer. Any sunlight obstructed by clouds will also obstruct the NO_2 both at the surface and in the full boundary layer.

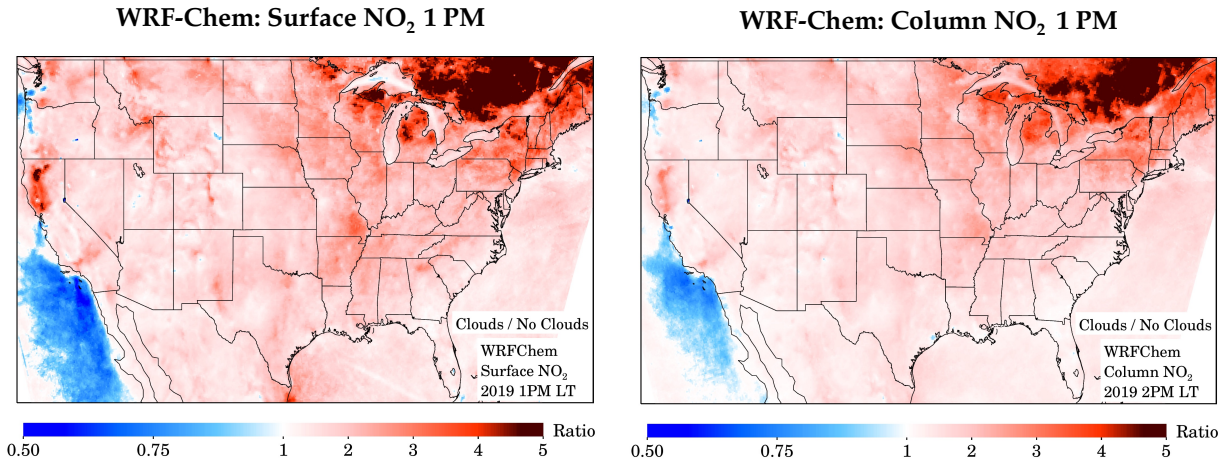

Figure 7. Ratio of the annualized surface NO_2 at 13:30 local time from WRF-Chem during cloudy and cloud free days. (Left) Surface NO_2 (Right) Tropospheric column NO_2.

3.5 Impacts of clouds on geostationary observations

Finally, we use provisional TEMPO NO_2 data, TROPOMI NO_2 data, and AQS NO_2 data from 2 August 2023 through 30 June 2024 to understand how the changes of NO_2 during clear and cloudy conditions may be altered at different hours of the day (Figure 8). In this analysis, the threshold between high quality and lower quality data for both satellite products is a cloud radiative fraction = 0.15. Any TEMPO NO_2 or TROPOMI NO_2 measurement with crf < 0.15 was assumed to be "clear sky", while all other measurements are assumed to be cloudy. Hours with low solar zenith angles (before 8:00 and after 16:00) have been excluded from this analysis. We find that the difference in surface NO_2 between clear and cloudy days is small in the early morning hours and increases throughout the day.

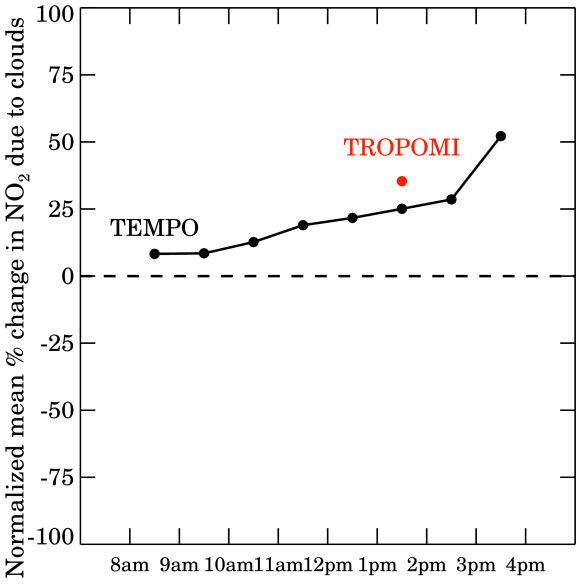

Figure 8. Normalized mean percentage change in the surface NO_2 during days with cloudy skies as opposed to days with clear skies. Red dot shows the mean percentage change using TROPOMI clouds as shown in Figure 2c. Black line uses the same procedure for Aug 2023 – June 2024 data and TEMPO cloud data.

Surface AQS NO_2 at 8:30 local time is +8.3% larger on cloudy days than clear sky days, while at 15:30 it is +52.2% larger. The calculated 13:30 difference in surface NO_2 between cloudy and clear sky days using TEMPO (+25.1%) is similar to the analogous value from TROPOMI (+35.4%). Differences between TEMPO and TROPOMI are expected because the cloud algorithms and instrument characteristics are different, even though the timeframe and cloud filter threshold used for this analysis are the same.

4 Discussion

In this project we quantify how NO_2 satellite data could be biased in estimating annualized surface NO_2 concentrations due to having high quality measurements only in the absence of clouds. We find that surface *in situ* NO_2 measurements are on average +17% on all days compared to restricting to clear sky days and +36% larger during cloudy days vs. clear sky days, with a wide distribution based on geographic region and proximity to roadway. Using the United States as a case study, we find the clear-sky bias to be largest in the Northeast U.S.; conversely, the clear-sky bias is smallest in the Southwest U.S. and near major roadways. In some areas of the urban Western U.S., Los Angeles and San Diego, we find that NO_2 is lower on cloudy days, but these instances are rare (13% of monitoring sites) and are driven by unique transport patterns on cloudy days. Transport patterns are a significant driver of the regional clear vs. cloudy sky differences of surface NO_2 concentrations. Although the analysis was computed for both TROPOMI and TEMPO data, it should be re-emphasized that the cloud algorithms used by both instruments are different. However, the qualitative finding that surface NO_2 differences between cloudy and clear conditions tend to be larger in the afternoon than morning is consistent with a hypothesis that active photochemistry during periods of stronger afternoon sunlight would cause this change.

This work also highlights how NO_2 concentrations are different on days when satellite instruments are not acquiring a valid measurement. Our initial hypothesis of NO_2 being consistently larger on cloudy days was only partially proven true. In many cases, surface NO_2 concentrations and column NO_2 are larger, but this is not always the case. This project demonstrates the balancing act of the reduced NO_2 + OH sink and local climatological patterns (wind speed/direction, PBL depth, etc.) driving surface NO_2 during cloudy conditions. Although one of the original goals of this study was to better gap-fill satellite tropospheric vertical column NO_2 measurements in the presence of clouds, ultimately, we were not comfortable doing this yet. Reliance on a model as a transfer standard to convert surface concentrations into column concentrations exhibited too many biases under cloudy conditions. WRF-Chem model simulations of surface NO_2 suggest that the clear-sky bias in WRF-Chem is on average much larger than the observed clear-sky bias: +59% on cloudy days vs. clear days for the model, and +36% for the AQS data. We hypothesized that errors in OH chemistry, NO_2 recycling speeds, and PBL mixing depths could all be contributing to this high bias. Future work should target these three research topics. Future work could also use a machine-learning approach to account for some of these model biases.

Another consideration with the interpretation of satellite measurements is the impact of lightning NOx, wildfire NOx, and aircraft NOx emissions, mostly staying aloft, which could be misinterpreted as surface NO_2

enhancements. While lightning NOx and wildfire NOx emissions are often screened out when applying a cloud filter because they occur in optically thick clouds/smoke, it is possible for the NO_2 to remain aloft for several days after the initial thunderstorm/fire and be observed during clear skies. An algorithm to detect and screen out downwind NO_2 attributed to upwind lightning NOx and wildfire NOx emissions could be especially helpful. At minimum, care should be taken during timeframes and regions where there are large pulses of these types of emissions, such as our findings during summer.

In some ways, the chosen year 2019 was an ideal year to conduct the analysis because it preceded the 2020 global pandemic and its nonlinear and lingering effects on air pollution. But in other ways, this year was less ideal because TROPOMI pixel sizes changed in August 2019 from 7×3.5 km^2 (~25 km^2) to 5.5×3.5 km^2 (~19 km^2) The fraction of clear-sky pixels likely increased by 1 – 2% after August 2019 as smaller pixel sizes can better "see around" clouds (Krijger et al., 2007). This probably did not meaningfully affect our analysis but is nonetheless a caveat of using 2019 data.

These results have repercussions for many applied studies that use satellite data to estimate surface NO_2 concentrations or NOx emissions. First, for studies that estimate surface concentrations, it is important to ingest surface NO_2 measurements during cloudy (and nighttime) conditions in some capacity in order to appropriately estimate 24-hour concentrations; most studies already do this. If one were to use the clear-sky satellite data coupled with only a chemical transport model as a transfer standard to convert the column measurement into a pseudo-surface "measurement", this would underestimate annualized NO_2 concentration in most places. Unfortunately, there are many global regions with few or no surface measurements, so this is an important consideration when estimating surface NO_2 in these regions. But even if one were to ingest surface NO_2 during cloudy conditions, the spatial patterns of surface NO_2 during cloudy conditions may be slightly different than implied by the clear-sky satellite data. For example, we find that NO_2 surface concentrations under cloudy conditions are much larger in the Northeast U.S. than the Southwest U.S., and a cloud-free satellite map does not capture this.

Second, for nitrogen oxide emissions estimates it is often assumed that anthropogenic emission rates are similar under cloudy and clear-sky conditions, but this is likely not the case in reality. Although we show that surface NO_2 concentrations are typically smaller under clear-skies, it is likely that anthropogenic NOx emissions are actually larger under regionwide clear-skies during summer and winter due to the moderating impact of clouds on surface temperature and subsequent impacts on heating-ventilation-air conditioning (HVAC) usage/emissions (Abel et al., 2017). If we were able to better independently estimate tropospheric vertical column NO_2 during cloudy conditions, perhaps this could be investigated in the future.

Lastly, as satellite-derived NO_2 applications increase over the coming years, it is important to document its successes and shortcomings. We see this project as a first-step towards better accounting for the clear-sky bias of satellite NO_2 data. While future NO_2 applications may use geostationary data, such as TEMPO, which may suffer from a similar bias depending on the hour of the day, an advantage of geostationary satellite data is the ability to use multiple measurements per day before and just after the clouds. It might be possible to isolate a two-hour window

(one with a cloud and one without) to get a better handle on the instantaneous versus long-term role of clouds affecting NO_2 concentrations.

This work also highlights the critical role that chemical transport models can play in satellite NO_2 applications. Errors in the model assumptions can hamstring many NO_2 applications. For example, using a model to infer NO_2 during cloudy conditions in the lack of clear-sky satellite data would yield significant errors. Therefore, future work should concurrently focus on acquiring and using sub-orbital measurements to diagnose errors related in simulating NO_2 in chemical transport models, so that they can be used as more robust transfer standards.

Data availability. TROPOMI NO_2 version 2.4 data (http://doi.org/10.5270/S5P-9bnp8q8) processed to 0.01° × 0.01° resolution (http://doi.org/10.5067/MKJG22GUOD34) and TEMPO NO_2 version 3 data (http://doi.org/10.5067/IS-40e/TEMPO/NO2_L3.003) can be freely downloaded from NASA Earthdata. EPA AQS surface NO_2 data can be downloaded from pre-generated files: https://aqs.epa.gov/aqsweb/airdata/download_files.html. ERA5 re-analysis hourly data on single levels (http://doi.org/10.24381/cds.adbb2d47) can be downloaded from Copernicus Climate Data Store (https://cds.climate.copernicus.eu/#!/home). NOAA SURFAD data can be downloaded from: https://gml.noaa.gov/grad/surfrad/sitepage.html . Output from the WRF-Chem simulation is available upon request. IDL code to process the data is available upon request.

Author contribution. D.G., A.C., S.K., and S.A. developed the project design. J.H. and C.L. set-up and conducted the WRF-Chem simulations. D.G downloaded and processed the TROPOMI NO_2, TEMPO NO_2, ERA5, and SURFRAD data and re-gridded all data to a standardized grid. M.O.N. helped to process the surface NO_2 data. D.G. developed all figures for the manuscript and wrote the paper. All authors edited the manuscript.

Competing interests. The contact author has declared that none of the authors have any competing interests.

Acknowledgments. Preparation of this manuscript was funded by grants from the NOAA GeoXO program (1305M323PNRMA0668) and the NASA Health and Air Quality Applied Sciences Team (HAQAST) (80NSSC21K0511). NOAA Cooperative Agreement (NA17OAR4320101 and NA22OAR4320151) funded C. Lyu and J. He. The WRF-Chem simulation was supported by NOAA's High Performance Computing Program. The authors would also like to thank Brian McDonald and Laura Judd for very helpful feedback during preparation of this manuscript.

Supporting Information. The supporting information includes: 1) a spatial plot of the annual average of days with total cloud fraction less 0.5 as simulated by WRF-Chem during 8 AM, 1 PM, and 5 PM local time, 2) scatterplots of various 2019 annual averages of surface NO_2 and TROPOMI NO_2 measurements, 3) jNO_2 from WRF-Chem and an intercomparison with the NOAA SURFRAD network, 4) Tables of "cloudy vs. all days" and "all days vs. no clouds" analogous to Table 1 which shows "cloudy vs. no clouds".

References

Abel, D. W., Holloway, T., Kladar, R. M., Meier, P., Ahl, D., Harkey, M., & Patz, J. (2017). Response of Power Plant Emissions to Ambient Temperature in the Eastern United States. *Environmental Science and Technology*, *51*(10), 5838–5846. https://doi.org/10.1021/acs.est.6b06201

Acker, S. J., Holloway, T., & Harkey, M. K. (2025, February 13). Satellite Detection of NO2 Distributions and Comparison with Ground-Based Concentrations. *EGUsphere*. https://doi.org/10.5194/egusphere-2025-226

Anenberg, S. C., Mohegh, A., Goldberg, D. L., Kerr, G. H., Brauer, M., Burkart, K., et al. (2022). Long-term trends in urban NO2 concentrations and associated paediatric asthma incidence: estimates from global datasets. *The Lancet Planetary Health*, *6*(1), e49–e58. https://doi.org/10.1016/S2542-5196(21)00255-2

Bechle, M. J., Millet, D. B., & Marshall, J. D. (2015). National Spatiotemporal Exposure Surface for NO2: Monthly Scaling of a Satellite-Derived Land-Use Regression, 2000-2010. *Environmental Science and Technology*, *49*(20), 12297–12305. https://doi.org/10.1021/acs.est.5b02882

Boersma, K. F., Eskes, H. J., Dirksen, R. J., Van Der A, R. J., Veefkind, J. P., Stammes, P., et al. (2011). An improved tropospheric NO2 column retrieval algorithm for the Ozone Monitoring Instrument. *Atmospheric Measurement Techniques*, *4*(9), 1905–1928. https://doi.org/10.5194/amt-4-1905-2011

Burnett, R. T., Stieb, D., Brook, J. R., Cakmak, S., Dales, R., Raizenne, M., et al. (2004). Associations between short-term changes in nitrogen dioxide and mortality in Canadian cities. *Archives of Environmental Health*, *59*(5), 228–236. https://doi.org/10.3200/AEOH.59.5.228-236

Busca, G., Lietti, L., Ramis, G., & Berti, F. (1998). Chemical and mechanistic aspects of the selective catalytic reduction of NO(x) by ammonia over oxide catalysts: A review. *Applied Catalysis B: Environmental*, *18*(1–2), 1–36. https://doi.org/10.1016/S0926-3373(98)00040-X

Cao, E. L. (2023). National ground-level NO2 predictions via satellite imagery driven convolutional neural networks. *Frontiers in Environmental Science*, *11*. https://doi.org/10.3389/fenvs.2023.1285471

Crippa, M., Guizzardi, D., Pisoni, E., Solazzo, E., Guion, A., Muntean, M., et al. (2021). Global anthropogenic emissions in urban areas: patterns, trends, and challenges. *Environmental Research Letters*, *16*(7), 074033. https://doi.org/10.1088/1748-9326/AC00E2

Demetillo, M. A. G., Navarro, A., Knowles, K. K., Fields, K. P., Geddes, J. A., Nowlan, C. R., et al. (2020). Observing Nitrogen Dioxide Air Pollution Inequality Using High-Spatial-Resolution Remote Sensing Measurements in Houston, Texas. *Environmental Science & Technology*, *54*(16), 9882–9895. https://doi.org/10.1021/acs.est.0c01864

Dickerson, R. R., Anderson, D. C., & Ren, X. (2019). On the use of data from commercial NOx analyzers for air pollution studies. *Atmospheric Environment*, *214*, 116873. https://doi.org/10.1016/j.atmosenv.2019.116873

Dressel, I. M., Demetillo, M. A. G., Judd, L. M., Janz, S. J., Fields, K. P., Sun, K., et al. (2022). Daily Satellite Observations of Nitrogen Dioxide Air Pollution Inequality in New York City, New York and Newark, New Jersey: Evaluation and Application. *Environmental Science and Technology*, *2022*. https://doi.org/10.1021/ACS.EST.2C02828/ASSET/IMAGES/LARGE/ES2C02828_0006.JPEG

Duncan, B. N., Anderson, D. C., Fiore, A. M., Joiner, J., Krotkov, N. A., Li, C., et al. (2024). Opinion: Beyond global means – novel space-based approaches to indirectly constrain the concentrations of and trends and

variations in the tropospheric hydroxyl radical (OH). *Atmospheric Chemistry and Physics*, *24*(22), 13001–13023. https://doi.org/10.5194/acp-24-13001-2024

Eskes, H., van Geffen, J., Boersma, F., Eichman, K., Apituley, A., Pedergnana, M., et al. (2022). *Sentinel-5 precursor/TROPOMI Level 2 Product User Manual Nitrogendioxide*.

de Foy, B., Krotkov, N. A., Bei, N., Herndon, S. C., Huey, L. G., Martínez, A.-P., et al. (2009). Hit from both sides: tracking industrial and volcanic plumes in Mexico City with surface measurements and OMI SO2 retrievals during the MILAGRO field campaign. *Atmospheric Chemistry and Physics*, *9*(24), 9599–9617. https://doi.org/10.5194/acp-9-9599-2009

Geddes, J. A., Murphy, J. G., O'Brien, J. M., & Celarier, E. A. (2012). Biases in long-term NO2 averages inferred from satellite observations due to cloud selection criteria. *Remote Sensing of Environment*, *124*(2), 210–216. https://doi.org/10.1016/j.rse.2012.05.008

van Geffen, J. (2016). TROPOMI ATBD of the total and tropospheric NO2 data products, (2). Retrieved from https://sentinel.esa.int/documents/247904/2476257/Sentinel-5P-TROPOMI-ATBD-NO2-data-products

van Geffen, J., Boersma, K. F., Eskes, H. J., Sneep, M., ter Linden, M., Zara, M., & Veefkind, J. P. (2020). S5P TROPOMI NO2 slant column retrieval: method, stability, uncertainties and comparisons with OMI. *Atmospheric Measurement Techniques*, *13*(3), 1315–1335. https://doi.org/10.5194/amt-13-1315-2020

van Geffen, J., Eskes, H. J., Compernolle, S., Pinardi, G., Verhoelst, T., Lambert, J.-C., et al. (2021). Sentinel-5P TROPOMI NO2 retrieval: impact of version v2.2 improvements and comparisons with OMI and ground-based data. *Atmospheric Measurement Techniques*, *15*(7), 2037–2060. https://doi.org/10.5194/AMT-15-2037-2022

Ghahremanloo, M., Lops, Y., Choi, Y., & Yeganeh, B. (2021). Deep Learning Estimation of Daily Ground-Level NO2 Concentrations From Remote Sensing Data. *Journal of Geophysical Research: Atmospheres*, *126*(21), e2021JD034925. https://doi.org/10.1029/2021JD034925

Ghahremanloo, M., Lops, Y., Choi, Y., Mousavinezhad, S., & Jung, J. (2023). A Coupled Deep Learning Model for Estimating Surface NO2 Levels from Remote Sensing Data: 15-Year Study Over the Contiguous United States. *Journal of Geophysical Research: Atmospheres*, e2022JD037010. https://doi.org/10.1029/2022JD037010

Glissenaar, I., Folkert Boersma, K., Anglou, I., Rijsdijk, P., Verhoelst, T., Compernolle, S., et al. (2025). TROPOMI Level 3 tropospheric NO2 Dataset with Advanced Uncertainty Analysis from the ESA CCI+ ECV Precursor Project. *EGUsphere*. https://doi.org/10.21944/CCI-NO2-TROPOMI-L3

Goldberg, D. L., Anenberg, S. C., Kerr, G. H., Mohegh, A., Lu, Z., & Streets, D. G. (2021). TROPOMI NO2 in the United States: A Detailed Look at the Annual Averages, Weekly Cycles, Effects of Temperature, and Correlation With Surface NO 2 Concentrations. *Earth's Future*, *9*(4), e2020EF001665. https://doi.org/10.1029/2020EF001665

Goldberg, D. L., Harkey, M., de Foy, B., Judd, L., Johnson, J., Yarwood, G., & Holloway, T. (2022). Evaluating NOx emissions and their effect on O3 production in Texas using TROPOMI NO2 and HCHO. *Atmospheric Chemistry and Physics*, *22*(16), 10875–10900. https://doi.org/10.5194/acp-22-10875-2022

Goldberg, D. L., Tao, M., Kerr, G. H., Ma, S., Tong, D. Q., Fiore, A. M., et al. (2024). Evaluating the spatial patterns of U.S. urban NOx emissions using TROPOMI NO2. *Remote Sensing of Environment*, *300*, 113917. https://doi.org/10.1016/j.rse.2023.113917

Harkey, M., & Holloway, T. (2024). Simulated Surface-Column NO2 Connections for Satellite Applications. *Journal of Geophysical Research: Atmospheres*, *129*(21). https://doi.org/10.1029/2024JD041912

He, J., Harkins, C., O'Dell, K., Li, M., Francoeur, C., Aikin, K. C., et al. (2024). COVID-19 perturbation on US air quality and human health impact assessment. *PNAS Nexus*, *3*(1). https://doi.org/10.1093/pnasnexus/pgad483

He, M. Z., Kinney, P. L., Li, T., Chen, C., Sun, Q., Ban, J., et al. (2020). Short- and intermediate-term exposure to NO2 and mortality: A multi-county analysis in China. *Environmental Pollution*, *261*, 114165. https://doi.org/10.1016/j.envpol.2020.114165

Health Effects Institute. (2022). *Systematic Review and Meta-analysis of Selected Health Effects of Long-Term Exposure to Traffic-Related Air Poll*. Retrieved from https://www.healtheffects.org/system/files/hei-special-report-23-executive-summary_0.pdf

Hegarty, J. D., Lewis, J., McGrath-Spangler, E. L., Henderson, J., Scarino, A. J., DeCola, P., et al. (2018). Analysis of the Planetary Boundary Layer Height during DISCOVER-AQ Baltimore–Washington, D.C., with Lidar and High-Resolution WRF Modeling. *Journal of Applied Meteorology and Climatology*, *57*(11), 2679–2696. https://doi.org/10.1175/JAMC-D-18-0014.1

Hersbach, H., Bell, B., Berrisford, P., Hirahara, S., Horányi, A., Muñoz-Sabater, J., et al. (2020). The ERA5 global reanalysis. *Quarterly Journal of the Royal Meteorological Society*, *146*(730), 1999–2049. https://doi.org/10.1002/qj.3803

Jin, X., Zhu, Q., & Cohen, R. C. (2021). Direct estimates of biomass burning NOx emissions and lifetimes using daily observations from TROPOMI. *Atmospheric Chemistry and Physics*, *21*(20), 15569–15587. https://doi.org/10.5194/acp-21-15569-2021

Kebabian, P. L., Wood, E. C., Herndon, S. C., & Freedman, A. (2008). A practical alternative to chemiluminescence-based detection of nitrogen dioxide: Cavity attenuated phase shift spectroscopy. *Environmental Science and Technology*, *42*(16), 6040–6045. https://doi.org/10.1021/es703204j

Kelly, K. E., Whitaker, J., Petty, A., Widmer, C., Dybwad, A., Sleeth, D., et al. (2017). Ambient and laboratory evaluation of a low-cost particulate matter sensor. *Environmental Pollution*, *221*, 491–500. https://doi.org/10.1016/j.envpol.2016.12.039

Kenagy, H. S., Sparks, T. L., Ebben, C. J., Wooldrige, P. J., Lopez-Hilfiker, F. D., Lee, B. H., et al. (2018). NOx Lifetime and NOy Partitioning During WINTER. *Journal of Geophysical Research: Atmospheres*, *123*(17), 9813–9827. https://doi.org/10.1029/2018JD028736

Kerr, G. H., Goldberg, D. L., Harris, M. H., Henderson, B. H., Hystad, P., Roy, A., & Anenberg, S. C. (2023). Ethnoracial Disparities in Nitrogen Dioxide Pollution in the United States: Comparing Data Sets from Satellites, Models, and Monitors. *Environmental Science & Technology*. https://doi.org/10.1021/acs.est.3c03999

Khreis, H., Kelly, C., Tate, J., Parslow, R., Lucas, K., & Nieuwenhuijsen, M. (2017). Exposure to traffic-related air pollution and risk of development of childhood asthma: A systematic review and meta-analysis. *Environment International*, *100*, 1–31. https://doi.org/10.1016/j.envint.2016.11.012

Kim, E. J., Holloway, T., Kokandakar, A., Harkey, M., Elkins, S., Goldberg, D. L., & Heck, C. (2024). A Comparison of Regression Methods for Inferring Near-Surface NO_2 With Satellite Data. *Journal of Geophysical Research: Atmospheres*, *129*(16). https://doi.org/10.1029/2024JD040906

Koltsakis, G., & Stamatelos, A. (1997). Catalytic automotive exhaust aftertreatment. *Progress in Energy and Combustion Science*, *23*(1), 1–39. https://doi.org/10.1016/s0360-1285(97)00003-8

Krijger, J. M., Van Weele, M., Aben, I., & Frey, R. (2007). *Atmospheric Chemistry and Physics Technical Note: The effect of sensor resolution on the number of cloud-free observations from space*. *Atmos. Chem. Phys* (Vol. 7). Retrieved from www.atmos-chem-phys.net/7/2881/2007/

Kuhn, L., Beirle, S., Kumar, V., Osipov, S., Pozzer, A., Bösch, T., et al. (2024). On the influence of vertical mixing, boundary layer schemes, and temporal emission profiles on tropospheric NO2 in WRF-Chem – comparisons to in situ, satellite, and MAX-DOAS observations. *Atmospheric Chemistry and Physics*, *24*(1), 185–217. https://doi.org/10.5194/acp-24-185-2024

Lambert, J.-C., Claas, J., Stein-Zweers, D., Ludewig, A., Loyola, D., Sneep, M., & Dehn, A. (2023). *Quarterly Validation Report of the Copernicus Sentinel-5 Precursor Operational Data Products #19*.

Lamsal, L. N., Martin, R. V., van Donkelaar, A., Steinbacher, M., Celarier, E. A., Bucsela, E. J., et al. (2008). Ground-level nitrogen dioxide concentrations inferred from the satellite-borne Ozone Monitoring Instrument. *Journal of Geophysical Research Atmospheres*, *113*(16), 1–15. https://doi.org/10.1029/2007JD009235

Larkin, A., Anenberg, S., Goldberg, D. L., Mohegh, A., Brauer, M., & Hystad, P. (2023). A global spatial-temporal land use regression model for nitrogen dioxide air pollution. *Frontiers in Environmental Science*, *11*, 484. https://doi.org/10.3389/FENVS.2023.1125979

Laughner, J. L., & Cohen, R. C. (2019). Direct observation of changing NOx lifetime in North American cities. *Science*, *366*(6466), 723–727. https://doi.org/10.1126/science.aax6832

Levelt, P. F., Joiner, J., Tamminen, J., Veefkind, J. P., Bhartia, P. K., Zweers, D. C. S., et al. (2018). The Ozone Monitoring Instrument: Overview of 14 years in space. *Atmospheric Chemistry and Physics*, *18*(8), 5699–5745. https://doi.org/10.5194/acp-18-5699-2018

Lin, M., Horowitz, L. W., Hu, L., & Permar, W. (2024). Reactive Nitrogen Partitioning Enhances the Contribution of Canadian Wildfire Plumes to US Ozone Air Quality. *Geophysical Research Letters*, *51*(15). https://doi.org/10.1029/2024GL109369

Liu, F., Beirle, S., Zhang, Q., Dörner, S., He, K., & Wagner, T. (2016). NOx lifetimes and emissions of cities and power plants in polluted background estimated by satellite observations. *Atmospheric Chemistry and Physics*, *16*(8), 5283–5298. https://doi.org/10.5194/acp-16-5283-2016

Liu, S., Valks, P., Pinardi, G., Xu, J., Chan, K. L., Argyrouli, A., et al. (2021). An improved TROPOMI tropospheric NO2 research product over Europe. *Atmospheric Measurement Techniques*, *14*(11), 7297–7327. https://doi.org/10.5194/amt-14-7297-2021

Liu, X., Wang, Y., Wasti, S., Li, W., Soleimanian, E., Flynn, J., et al. (2023). Evaluating WRF-GC v2.0 predictions of boundary layer height and vertical ozone profile during the 2021 TRACER-AQ campaign in Houston, Texas. *Geoscientific Model Development*, *16*(18), 5493–5514. https://doi.org/10.5194/gmd-16-5493-2023

Lorente, A., Folkert Boersma, K., Yu, H., Dörner, S., Hilboll, A., Richter, A., et al. (2017). Structural uncertainty in air mass factor calculation for NO2 and HCHO satellite retrievals. *Atmospheric Measurement Techniques*, *10*(3), 759–782. https://doi.org/10.5194/amt-10-759-2017

Martin, R. V., Brauer, M., van Donkelaar, A., Shaddick, G., Narain, U., & Dey, S. (2019). No one knows which city has the highest concentration of fine particulate matter. *Atmospheric Environment: X*, 100040. https://doi.org/10.1016/J.AEAOA.2019.100040

Maruhashi, J., Mertens, M., Grewe, V., & Dedoussi, I. C. (2024). A multi-method assessment of the regional sensitivities between flight altitude and short-term O3 climate warming from aircraft NOx emissions. *Environmental Research Letters*. https://doi.org/10.1088/1748-9326/ad376a

Nault, B. A., Laughner, J. L., Wooldridge, P. J., Crounse, J. D., Dibb, J., Diskin, G., et al. (2017). Lightning NOx Emissions: Reconciling Measured and Modeled Estimates With Updated NOx Chemistry. *Geophysical Research Letters*, *44*(18), 9479–9488. https://doi.org/10.1002/2017GL074436

Nawaz, M. O., Goldberg, D. L., Kerr, G. H., & Anenberg, S. C. (2025). TROPOMI Satellite Data Reshape NO2 Air Pollution Land-Use Regression Modeling Capabilities in the United States. *ACS ES&T Air*. https://doi.org/10.1021/acsestair.4c00153

Nowlan, C. R., Abad, G. G., Liu, X., Wang, H., & Chance, K. (2025). TEMPO Nitrogen Dioxide Retrieval Algorithm Theoretical Basis Document. https://doi.org/10.5067/WX026254FI2U

Palmer, P. I., Jacob, D. J., Chance, K. V., Martin, R. V., Spurr, R. J. D., Kurosu, T. P., et al. (2001). Air mass factor formulation for spectroscopic measurements from satellites: Application to formaldehyde retrievals from the Global Ozone Monitoring Experiment. *Journal of Geophysical Research: Atmospheres*, *106*(D13), 14539–14550. https://doi.org/10.1029/2000JD900772

Platt, U. (1994). Differential Optical Absorption Spectroscopy (DOAS). In *Air monitoring by spectroscopic techniques* (p. 531). Wiley-IEEE.

Poraicu, C., Müller, J.-F., Stavrakou, T., Fonteyn, D., Tack, F., Deutsch, F., et al. (2023). Cross-evaluating WRF-Chem v4.1.2, TROPOMI, APEX, and in situ NO2 measurements over Antwerp, Belgium. *Geosci. Model Dev*, *16*, 479–508. https://doi.org/10.5194/gmd-16-479-2023

Rijsdijk, P., Eskes, H., Dingemans, A., Boersma, K. F., Sekiya, T., Miyazaki, K., & Houweling, S. (2025). Quantifying uncertainties in satellite NO2 superobservations for data assimilation and model evaluation. *Geoscientific Model Development*, *18*(2), 483–509. https://doi.org/10.5194/gmd-18-483-2025

Ryu, Y. H., Hodzic, A., Barre, J., Descombes, G., & Minnis, P. (2018). Quantifying errors in surface ozone predictions associated with clouds over the CONUS: A WRF-Chem modeling study using satellite cloud retrievals. *Atmospheric Chemistry and Physics*, *18*(10), 7509–7525. https://doi.org/10.5194/acp-18-7509-2018

Sarwar, G., Hogrefe, C., Henderson, B. H., Mathur, R., Gilliam, R., Callaghan, A. B., et al. (2024). Impact of particulate nitrate photolysis on air quality over the Northern Hemisphere. *Science of The Total Environment*, *917*, 170406. https://doi.org/10.1016/j.scitotenv.2024.170406

Shah, V., Jacob, D. J., Li, K., Silvern, R. F., Zhai, S., Liu, M., et al. (2020). Effect of changing NOx lifetime on the seasonality and long-term trends of satellite-observed tropospheric NO2 columns over China. *Atmospheric Chemistry and Physics Discussions*, *20*(3), 1483–1495. https://doi.org/10.5194/acp-2019-670

Shah, V., Keller, C. A., Knowland, K. E., Christiansen, A., Hu, L., Wang, H., et al. (2024). Particulate Nitrate Photolysis as a Possible Driver of Rising Tropospheric Ozone. *Geophysical Research Letters*, *51*(5). https://doi.org/10.1029/2023GL107980

Shetty, S., Schneider, P., Stebel, K., David Hamer, P., Kylling, A., & Koren Berntsen, T. (2024). Estimating surface NO2 concentrations over Europe using Sentinel-5P TROPOMI observations and Machine Learning. *Remote Sensing of Environment*, *312*, 114321. https://doi.org/10.1016/j.rse.2024.114321

Sullivan, D. M., & Krupnick, A. (2018). *Using Satellite Data to Fill the Gaps in the US Air Pollution Monitoring Network*. NW. Retrieved from https://www.rff.org/publications/working-papers/using-satellite-data-to-fill-the-gaps-in-the-us-air-pollution-monitoring-network/

Sun, K., Zhu, L., Cady-Pereira, K. E., Chan Miller, C., Chance, K. V., Clarisse, L., et al. (2018). A physics-based approach to oversample multi-satellite, multi-species observations to a common grid. *Atmospheric Measurement Techniques Discussions*, *11*(12), 1–30. https://doi.org/10.5194/amt-2018-253

Sun, W., Tack, F., Clarisse, L., Schneider, R., Stavrakou, T., & Van Roozendael, M. (2024). Inferring Surface NO2 Over Western Europe: A Machine Learning Approach With Uncertainty Quantification. *Journal of Geophysical Research: Atmospheres*, *129*(20). https://doi.org/10.1029/2023JD040676

Thornton, J. A., Wooldridge, P. J., & Cohen, R. C. (2000). Atmospheric NO2: In Situ Laser-Induced Fluorescence Detection at Parts per Trillion Mixing Ratios. *Analytical Chemistry*, *72*(3), 528–539. https://doi.org/10.1021/ac9908905

Vandaele, A. C., Hermans, C., Simon, P. C., Carleer, M., Colin, R., Fally, S., et al. (1998). Measurements of the NO2 absorption cross-section from 42 000 cm−1 to 10 000 cm−1 (238–1000 nm) at 220 K and 294 K. *Journal of Quantitative Spectroscopy and Radiative Transfer*, *59*(3–5), 171–184. https://doi.org/10.1016/S0022-4073(97)00168-4

Veefkind, J. P., Aben, I., McMullan, K., Förster, H., de Vries, J., Otter, G., et al. (2012). TROPOMI on the ESA Sentinel-5 Precursor: A GMES mission for global observations of the atmospheric composition for climate, air quality and ozone layer applications. *Remote Sensing of Environment*, *120*(2012), 70–83. https://doi.org/10.1016/j.rse.2011.09.027

Zare, A., Romer, P. S., Nguyen, T., Keutsch, F. N., Skog, K., & Cohen, R. C. (2018). A comprehensive organic nitrate chemistry: Insights into the lifetime of atmospheric organic nitrates. *Atmospheric Chemistry and Physics*, *18*(20), 15419–15436. https://doi.org/10.5194/acp-18-15419-2018